Journal Pre-proofs

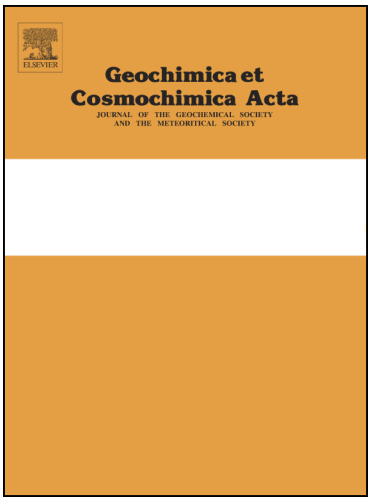

Experimental partitioning of osmium between pyrite and fluid: constraints on the mid-ocean ridge hydrothermal flux of osmium to seawater

Drew D. Syverson, Joachim A.R. Katchinoff, Laurel R. Yohe, Benjamin M. Tutolo, William E. Seyfried Jr., Alan D. Rooney

PII: S0016-7037(20)30663-3
DOI: https://doi.org/10.1016/j.gca.2020.10.029
Reference: GCA 11973

To appear in: *Geochimica et Cosmochimica Acta*

Received Date: 3 May 2020
Revised Date: 22 October 2020
Accepted Date: 27 October 2020

Please cite this article as: Syverson, D.D., Katchinoff, J.A.R., Yohe, L.R., Tutolo, B.M., Seyfried, W.E. Jr., Rooney, A.D., Experimental partitioning of osmium between pyrite and fluid: constraints on the mid-ocean ridge hydrothermal flux of osmium to seawater, *Geochimica et Cosmochimica Acta* (2020), doi: https://doi.org/10.1016/j.gca.2020.10.029

Experimental partitioning of osmium between pyrite and fluid: constraints on the mid-ocean ridge hydrothermal flux of osmium to seawater

*[1]Drew D. Syverson, [1]Joachim A.R. Katchinoff, [1]Laurel R. Yohe,

[2]Benjamin M. Tutolo, [3]William E. Seyfried, Jr., [1]Alan D. Rooney

[1]Yale University, Department of Earth and Planetary Sciences, New Haven, CT, USA

[2]University of Calgary, Department of Geoscience, Calgary, AB, CA

[3]University of Minnesota, Department of Earth and Environmental Sciences, Minneapolis, MN, USA

*Corresponding author: syverson.drew@gmail.com

Phone Number: +1 612-475-0575

Abstract

This study presents experimental, geochemical modeling, and field data focusing on the partitioning of osmium (Os) between fluid and pyrite upon precipitation at conditions representative of mid-ocean ridge hydrothermal environments. Dissolved Os partitions strongly into pyrite upon precipitation at experimental conditions, 350°C and 50 MPa, with a representative relative Os/Fe partition coefficient, $D_{Pyrite-Fluid}^{Os/Fe}$, between 10 and 15. Integrating the experimentally determined $D_{Pyrite-Fluid}^{Os/Fe}$ into a geochemical model indicates that a significant amount of Os is retained within the subseafloor due to sulfide precipitation induced by mixing of conductively heated seawater with pristine high temperature hydrothermal fluids that are enriched in dissolved metals, such as Os and Fe. Comparison with existing Os concentration and isotopic data of

hydrothermal fluids and sulfide minerals from a wide range of hydrothermal systems with the experimental and modeling constraints suggest that modern high temperature hydrothermal systems are a minor source of unradiogenic Os to the modern global ocean dissolved Os budget due to the majority of Os being sequestered into sulfide minerals formed within and on the seafloor.

1. Introduction

The platinum group element[1] osmium (Os), and associated isotope ratios $^{187}Os/^{188}Os$ and $^{186}Os/^{188}Os$, have been used to decipher the co-evolution of the mantle and crust, the silicate-CO_2 weathering feedback throughout Earth's history, and the timing and mechanisms controlling ore genesis in magmatic systems (Brandon et al., 1996; Brenan et al., 2016; Carlson, 2005; Nozaki et al., 2013; Oxburgh et al., 2007; Peucker-Ehrenbrink et al., 2003; Ravizza et al., 2001b; Selby and Creaser, 2004; Sharma et al., 2007; Stein et al., 2000). However, the partitioning of Os into fluids during water-rock interaction and upon formation of sulfide minerals is poorly constrained, especially at hydrothermal conditions relevant to mid-ocean ridge (MOR) hydrothermal environments (Brügmann et al., 1998; Ravizza et al., 1996; Sharma et al., 2007; Sharma et al., 2000; Zeng et al., 2014). Due to the highly siderophile and chalcophile nature of Os, the process of sulfide mineral formation will have a significant effect on the mobility of Os in the source hydrothermal fluids. The precipitation of such sulfides will have a direct effect on the overall flux of Os to the oceans resulting in distinct Os concentrations and isotopic reservoirs. This process is apparent but our understanding regarding the magnitude of Os partitioning between sulfide minerals and hydrothermal fluids is limited in part by the dearth of existing experimental studies exploring Os solubility at a range of pertinent physiochemical conditions (Foustoukos, 2019; Foustoukos et al., 2015; Xiong and Wood, 2000).

[1] Platinum group elements (PGE): Os, Ir, Ru, Rh, Pt, and Pd

A significant range of physiochemical conditions exists within the subseafloor of MOR hydrothermal environments. During alteration of oceanic crust (~200-400°C, 30-70 MPa), the hydrolysis and oxidation of Fe^{2+}-bearing silicate and sulfide minerals results in the production of H_2 and reduction of seawater-derived SO_4^{2-} to H_2S, creating a large range in O_2 and S_2 fugacity, *i.e.*, range in the activities of dissolved H_2 and H_2S/SO_4^{2-} (German and Seyfried, 2014). Osmium, which is initially retained in primary magmatic base metal sulfide minerals, such as pentlandite $(Fe,Ni)_9S_8$, will become liberated into fluids upon hydrothermal alteration of primary sulfide minerals to secondary sulfides in tandem with subsolidus phase transformations, such as exsolution of PGE sulfide minerals and/or refractory Pt-Fe alloys (Foustoukos, 2019; Foustoukos et al., 2015). These processes are apparent from natural observations of secondary sulfides and alloys in exhumed abyssal peridotites (Carlson, 2005). However, the experimental determination of the solid-solution systematics dictating the solubility of Os partitioning into sulfides, the reaction kinetics and mechanisms responsible for Os mass transfer, and the fluid chemistry controls all remain largely unexplored (Sun and Ceder, 2011; Xiong and Wood, 2000). The lack of understanding of the partitioning of Os between primary and secondary sulfide minerals and fluids limits our ability to predict the mobilization of Os during a number of processes, such as the dehydration of the subducted oceanic crust that ultimately results in mantle metasomatism or the formation of massive sulfides within the oceanic crust along Earth's MOR system. Elucidating these processes will provide much needed constraints on Os behavior and cycling in the Earth system, with the potential to address issues with the modern Os mass balance and the application of Os isotope stratigraphy as a paleoweathering proxy (Cohen et al., 2004; Oxburgh et al., 2007;

Paquay and Ravizza, 2012a; Paquay and Ravizza, 2012b; Ravizza et al., 2001a; Rooney et al., 2016; Sharma et al., 2007).

In order to more fully understand the geochemical behavior of Os under hydrothermal conditions and to address extant geochemical uncertainties, this study focuses on the experimental examination of Os partitioning between pyrite and fluid at temperature, pressure, and chemical conditions relevant to massive sulfide formation within the subseafloor of MOR hydrothermal systems. Pyrite is ubiquitous in MOR hydrothermal systems and has been proposed to be the predominant sulfide mineral responsible for sequestering Os from hydrothermal fluids. Data from this study provides the first experimental constraints on the fate of Os derived from the oceanic crust upon the precipitation of pyrite in high temperature, subseafloor hydrothermal systems. To provide a process-oriented perspective on Os partitioning, this study also couples the experimentally determined pyrite-fluid Os partitioning data with thermodynamic modeling simulations to describe the extent of sulfide precipitation in the subseafloor upon mixing conductively heated seawater with pristine hydrothermal fluids derived from the deep subseafloor. In turn, these simulations enable the estimation of the amount of dissolved Os removed via pyrite precipitation in natural MOR systems.

2. Methods

2.1 Experimental Design

Two high temperature hydrothermal experiments were conducted to provide an experimental blank and to simulate the partitioning of Os between pyrite and fluid upon pyrite precipitation at conditions representative of chemical reactions occurring in the subseafloor at MORs. Following

recent studies in the pyrite-fluid system (Syverson et al., 2013; Syverson et al., 2015), the hydrothermal experiments utilized gold-cell reactor technology (Seyfried et al., 1987). The experimental blank (Expt. #0) was conducted to assess the contribution of Fe and Os derived from the reactor assembly upon reaction with the reactant solution, where the initial reactor solution contained 1000 mmol/kg NaCl solution at an acidic $pH_{25°C} \approx 1$. The acidic pH and high dissolved Cl^- concentration were used to enhance the solubility of metals at experimental conditions. Importantly, efforts were made to avoid contamination of the "blank run" by delaying preparation of the Os-rich (reaction fluid) until the blank run had been completed (Table 1). The blank solution was loaded into the gold cell reactor, sealed in the high-pressure autoclave, and heated to 350°C, isobarically at 50 MPa. The reactor was allowed to remain at conditions for 24 hours and then the reactor solution was sampled at *in-situ* conditions. Afterward, the reactor was cooled to ambient laboratory conditions. The pyrite precipitation experiment (Expt. #1), used the same gold-cell reactor and Ti-capillary tubing and valves as the blank experiment, all of which were cleaned with 11.8 and 0.1 M trace-element grade HCl, respectively. Experiment #1 is similar in design as the experiments performed by Syverson et al. (2013) and Syverson et al. (2015), where the precipitation of pyrite was induced by the introduction of a S-bearing solution at experimental pressure and temperature conditions into the acidic Fe^{2+}- Os- and Cl-bearing reactor solution. The reactant solution used for Expt. #1 was enriched in dissolved Os, 2 μmol/kg, significantly greater compared to natural concentrations (Ravizza et al., 1996; Roy-Barman and Allègre, 1994). The Os solution used for the pyrite precipitation experiment was the commercially-available reference solution: Durham Romil Osmium Solution (DROsS; http://iageo.com/dross-os-isotope-reference-solution/) (Luguet et al., 2008; Nowell et al., 2008) (Table 1). The elevated dissolved Os concentration in the reactant solution was prescribed to provide a sufficient amount of dissolved

Os to remain after pyrite precipitation and recrystallization and thereby permit precise quantification of Os partitioning between pyrite and dissolved Os-species.

Specifically, an enriched 39 mmol/kg Fe- and 2 μmol/kg Os-bearing acidic 1000 mmol/kg NaCl solution, with a $pH_{25°C} \approx 1$, was loaded and sealed into the gold-cell reactor assembly, sealed within the autoclave pressure vessel, and heated isobarically, at 50 MPa, to experimental conditions (Table 1). Upon reaching 350°C and 50 MPa, the homogeneous reactor solution was sampled to provide constraints on the initial solution chemistry of the reactor solution prior to the pyrite precipitation event. After this initial sample, a 1 mol/kg Na-thiosulfate ($Na_2S_2O_3$) solution was injected into the gold-cell reactor solution. Na-thiosulfate disproportionates at these temperature and chemical conditions, to H_2S and HSO_4^- at a 1:1 ratio, as follows:

$$S_2O_3^{2-} + H_2O + H^+ = H_2S + HSO_4^- \quad (1)$$

The transition in oxidation state of the experimental system and the presence of dissolved sulfur-species, H_2S and HSO_4^-, which both react with dissolved Fe^{2+}, induce the formation of pyrite:

$$1.75\ H_2S + 0.25\ HSO_4^- + Fe^{2+} = FeS_2 + 1.75\ H^+ + H_2O \quad (2)$$

The acidic pH and composition of the S-bearing solution were designed such that pyrite was the sole Fe-bearing mineral formed in the experiment to effectively limit the degree of freedom of Os partitioning to only be between the pyrite and fluid reservoirs. The concentration of dissolved Os in the reactor solution was monitored before and after the pyrite precipitation event to quantify the

degree of partitioning between pyrite and hydrothermal fluid upon precipitation and recrystallization and to account for the complete Fe and Os mass balance of the experimental system. After experiment termination, the product pyrite was recovered from the gold-cell reactor for determination of the Os concentration, which permitted verification of the integrity of mass balance within the experimental system.

2.2 Solution Chemistry Analysis and Characterization of Pyrite Product

The concentration of Fe^{2+} and the dissolved S-species, H_2S and SO_4^{2-}, were measured by use of a Thermo Scientific™ Element™ inductively coupled plasma mass spectrometry (ICP-MS) and by gravimetric methods, respectively. The relative standard deviation (2σ) for the determination of the concentration of dissolved Fe^{2+} by ICP-MS was ±1%. The concentration of H_2S was determined by taking a specific aliquot of the experimental solution into a pre-weighed gas-tight syringe, which was then weighed after sampling and subsequently injected into a N_2 glass-sparging system containing 5% phosphoric acid. This step liberates H_2S into the gas phase; this gas mixture is then transferred by bubbling into a $AgNO_3$ solution, which effectively traps the H_2S as solid Ag_2S. The remaining solution, sample + phosphoric acid, after sparging for a duration greater than one hour, was removed and mixed with a $BaCl_2$ solution to precipitate $BaSO_4$. Both Ag_2S and $BaSO_4$ were filtered from solution, washed with ultra-pure H_2O (18.2 MΩ/cm), dried, and weighed (see Syverson et al. (2015) for further details on methodology). The relative standard deviation associated with the H_2S and SO_4^{2-} measurements from gravimetric determination was ± 3%. The pH of the experimental solution samples was conducted by use of a Ross micro-electrode, which was calibrated with pH 4, 7, and 10 pH buffers, with an associated uncertainty of ± 0.02 pH units.

Characterization of the pyrite precipitate recovered after termination of Expt. #1 was performed by utilization of scanning electron microscopy (SEM), Raman spectroscopy, and energy-dispersive spectroscopy (EDS). The SEM images were produced by using a XL-30 Environmental SEM in secondary electron mode using a 10 kV accelerating voltage on product pyrite formed from the precipitation experiment to determine the morphology and grain size distribution. The pyrite precipitate was analyzed via Raman spectroscopy and EMPA/EDS at the University of Calgary. The Raman analysis was performed directly on the precipitate recovered from the experiment using a Horiba XPlora Plus instrument with a 50× objective and 785 nm laser at 1%, with 1200 gratings/cm on the detector. Thirty separate 40 s accumulations were acquired. Subsequently, the pyrite was embedded in epoxy and polished for SEM imaging and analysis. Back-scattered electron (BSE) imaging and EDS measurements were acquired on this polished sample using a JEOL JXA 8200 electron microprobe outfitted with a Bruker Energy Dispersive Spectrometer (EDS) at the University of Calgary.

2.3 Osmium Concentration and Isotope Analyses

Osmium isotope and elemental abundance analyses were performed on sulfide precipitates and solutions after retrieval from the gold cell reactor. In brief, between 0.2 and 0.5 g of sample together with a tracer enriched in ^{185}Re and ^{190}Os were weighed into borosilicate Carius tubes and digested using inverse aqua-regia (6 ml of 15M HNO_3 and 3 ml 12M HCl) at 220 °C for 48 hrs (Shirey and Walker, 1995). Osmium was isolated using solvent extraction ($CHCl_3$) and further purified using micro-distillation (Birck et al., 1997; Cohen and Waters, 1996). All Os isotopic measurements were determined by negative thermal ionization mass spectrometry (N-TIMS) (Creaser et al., 1991; Völkening et al., 1991) at the Yale Geochemistry and Geochronology Center.

The purified Os fractions were loaded onto Pt filaments together with an activator solution of $Ba(OH)_2$ in 0.1 M NaOH and analyzed using a Thermo Scientific Triton-Plus multi-collector TIMS via ion-counting using a secondary electron multiplier in peak-hopping mode. Interference of $^{187}ReO_3$ on $^{187}OsO_3$ was corrected by the measured intensity of $^{185}ReO_3$. Mass fractionation was corrected with $^{192}Os/^{188}Os = 3.083$, using an exponential fractional law. Total Os procedural blanks during this study were 0.1 ± 0.05 pg (1 S.D., $n = 4$), with an average $^{187}Os/^{188}Os$ value of 0.17 ± 0.15 ($n = 4$). Potential interferences for Os analyzed on the TIMS occur at masses: 234 ($^{186}WO_3$); 235 ($^{187}ReO_3$); 238 ($^{190}PtO_3$) and; 240 ($^{192}PtO_3$). To monitor for interference of Re on mass 235 (^{187}Os in our expectation) the ratio of 233/236 ($^{185}Re^{16}O_3/^{188}Os^{16}O_3$) was measured and was consistently 10^{-5} counts per second on the secondary electron multiplier. The two Pt interferences were monitored using 243 ($^{195}PtO3$) and were below detection for the secondary electron multiplier. Interference from tungsten ($^{186}WO_3$) was monitored using the mass for $^{183}WO_3$ and again, was below 10^{-5} cps at analytical conditions. Uncertainties for the $^{187}Os/^{188}Os$ were determined by propagation of all uncertainties in Os mass spectrometer measurements, blank abundances and isotopic compositions, spike calibrations and reproducibility of standard Os isotopic values. As a monitor of mass spectrometry reproducibility, an in-house Os standard solution was analyzed. For this analytical session the Os isotope standard, DROsS, yields an average $^{187}Os/^{188}Os$ ratio of 0.16103 ± 0.00019 (2 S.D., $n = 7$), in excellent agreement with previous studies (Nowell et al., 2008; Rooney et al., 2010).

To have a direct comparison with MOR vent sulfide minerals, this study also reports the Os concentration and isotope composition of sulfide minerals sampled from the interior of an active high temperature hydrothermal sulfide chimney, P-vent, which is located at a depth of

approximately 2516 meters on the seafloor along the fast-spreading East Pacific Rise within the 9°N hydrothermal system (EPR 9°50'N) (Fig. 1a). The chimney was recovered via the human operated vehicle (HOV) *Alvin* on the AT42-06 cruise aboard the R/V *Atlantis* in December 2018 (ALV 5009). Upon sampling, the vent fluid at P-vent was billowing black smoker precipitate into the overlying hydrothermal-seawater plume and had a temperature of 355°C. Aboard ship, the chimney sulfide was washed with ultra-pure H_2O and immediately dried under N_2. For Os concentration and $^{187}Os/^{188}Os$ analysis, sulfide was sampled from the interior of the chimney (Figs. 1b-c) and analyzed by X-ray diffraction, which indicated that the sulfide sample was predominantly chalcopyrite, and then preserved for subsequent LL-TIMS analysis, following the procedures used for experimental samples and standards.

2.4 Os/Fe Pyrite-Fluid Partitioning Systematics

Through solid-solution mixing by substitution of trace OsS_2 with the major disulfide-mineral endmember, pyrite (FeS_2), the distribution of Os and Fe between pyrite and hydrothermal fluid is described through the exchange reaction:

$$OsS_2 + Fe^{2+}(aq) = FeS_2 + Os^{2+}(aq) \quad (3)$$

The speciation of dissolved Os remains largely unconstrained, especially at hydrothermal conditions. However, an important constraint is provided through experimental Os solubility measurements performed by Xiong and Wood (2000) at conditions representative of porphyry and MOR hydrothermal environments. This particular study examined Os concentration measurements of hydrothermal fluid in the presence of Os-bearing minerals, such as OsS_2, at a range of redox

conditions and dissolved Cl^- contents, which overall show that Os^{2+} is the predominant oxidation state and is likely complexed to Cl^- in octahedral coordination (Brugger et al., 2016). There is currently no experimental data and there are only limited theoretical predictions that provide constraints on the solubility of Os in pyrite (Sun and Ceder, 2011). Given the oxidation state of osmium (Os^{2+}) in Cl- and S-bearing hydrothermal fluid and redox constraints necessary for pyrite formation, it is assumed that trace quantities of OsS_2 (<1 mol %) directly substitute for FeS_2. Speciation of the hydrothermal fluid was conducted to determine the Os-mineral stabilities between OsS_2, OsO_2, and Os, as described in section 2.5.

With regards to the Os/Fe exchange reaction, Equation 3, the partition coefficient $D_{Os/Fe}^{Pyrite}$ is calculated through the logarithmic Doerner-Hoskins relationship, which is representative of surface equilibrium upon growth from a compositionally evolving fluid, without internal reorganization of the crystal lattice within the time scale of the precipitation event (Doerner and Hoskins, 1925). Specifically, $D_{Os/Fe}^{Pyrite}$ was calculated through time-series measurement of the experimental change in dissolved Os and Fe concentration upon rapid precipitation of pyrite, as follows:

$$\log\left(\frac{[\mathrm{Os}]_{\mathrm{Fluid}}}{[\mathrm{Os}]_{\mathrm{Initial}}}\right) = D_{Os/Fe}^{Pyrite} \bullet \log\left(\frac{[\mathrm{Fe}]_{\mathrm{Fluid}}}{[\mathrm{Fe}]_{\mathrm{Initial}}}\right) \qquad (4)$$

For Equation 4, the initial Os and Fe concentration, prior to pyrite precipitation, was represented as $[Os]_{Initial}$ and $[Fe]_{Initial}$, respectively, and the concentration of Os and Fe after the pyrite precipitation event was represented as $[Os]_{Fluid}$ and $[Fe]_{Fluid}$, respectively.

The Doerner-Hoskins relationship is commonly used to characterize trace element partitioning upon irreversible co-precipitation that occurs at far-from equilibrium conditions, such as dissolved Os and Fe removal upon rapid sulfide precipitation. This partition coefficient has similarly been determined for other solid-aqueous solution systems, such as for describing Sr/Ca partitioning between anhydrite and hydrothermal fluids at MOR hydrothermal environments (Berndt et al., 1988; Mills et al., 1998; Shikazono and Holland, 1983). This trace-to-major element partition coefficient is different than the absolute partition coefficient commonly used for thermodynamic equilibrium partitioning of PGE at magmatic conditions (Fleet et al., 1996). Rather, the trace-to-major element partition coefficient is commonly utilized where the major element can be used to describe a process variable, such as dissolved Fe to describe the extent of Fe-sulfide mineralization in the subseafloor.

2.5 Geochemical Modeling

Thermodynamic modeling was conducted to assess the speciation and saturation state of the experimental fluids relative to Fe-Os-S-O minerals though utilization of the Geochemist Workbench (GWB) thermodynamic modeling program (Bethke et al., 2018). Additionally, GWB was used for thermodynamic simulations of the process of conductively heating seawater and mixing with high-temperature Fe- and Os-bearing hydrothermal fluid (the GWB modeling script is available within the Supplementary Information files). The speciation calculations and simulations were conducted by use of a thermodynamic database created using the DBCreate software (Kong et al., 2013) and is consistent with the framework of the Helgeson-Kirkham-Flowers (HKF) equation of state and with modifications thereafter (Helgeson et al., 1981; Shock et al., 1989; Shock et al., 1992; Shock et al., 1997; Sverjensky et al., 1997; Tanger and Helgeson,

1988). Additionally, the Os activity diagram was produced by combining thermodynamic data for the Os minerals Os, OsO_2, and OsS_2 (Knacke et al., 1991) with the thermodynamic properties of H_2S(aq) and H_2(aq) calculated using the SUPCRT92 thermodynamic data set.

The thermodynamic simulations were conducted by performing a series of systematic changes in the mass mixing ratio of conductively heated seawater (SW) relative to pristine end-member hydrothermal fluid (HF), SW:HF, at chemical and physical conditions representative of modern MOR hydrothermal systems. The thermodynamic simulations were performed isobarically at 50 MPa and result in a large a range of temperature and chemical conditions, which allowed for an assessment of the amount of pyrite precipitation that may occur in the subseafloor during this physiochemical process.

The first stage of the model simulates conductive heating of seawater to 250°C, which is a typical temperature determined from fluid inclusion thermometry and by mixing temperatures determined by the $^{87}Sr/^{86}Sr$ composition of anhydrite sampled from the subseafloor of MOR hydrothermal systems (Mills and Tivey, 1999; Palmer, 1992; Petersen et al., 1998; Shikazono and Holland, 1983; Teagle et al., 1998; Tivey et al., 1998). During this stage of the simulation, precipitation of anhydrite occurs and results in the modification of the fluid chemistry, in particular, the removal of seawater-derived Ca^{2+} and SO_4^{2-} due to the retrograde solubility of anhydrite ($CaSO_4$) (Blount and Dickson, 1969; Newton and Manning, 2005).

The second stage of the model involves mixing the homogenous, conductively-heated seawater with high temperature hydrothermal fluid, initially at 400°C, which is reducing and composed of

dissolved Fe^{2+} and H_2S at concentrations inferred to be representative of pristine end-member MOR hydrothermal fluid (*i.e.* without sulfide precipitate effects) from basalt-hosted systems (Seewald and Seyfried, 1990; Seyfried and Ding, 1993; Seyfried et al., 2011). The composition of the hydrothermal fluid was fixed as follows: NaCl, Fe^{2+}, H_2S, Ca^{2+}, Mg^{2+}, and H_2(aq) at concentrations of 550, 4, 17, 40, 0, and 2 mmol/kg, respectively, with an *in-situ* pH at 400°C of 5.0 (see Table S1). A range of SW:HF mass mixing ratios were used for the model simulations that encompass the range observed in natural systems, as indicated by the $^{87}Sr/^{86}Sr$ composition of sampled end-member hydrothermal fluids from modern MOR hydrothermal systems (Palmer, 1992; Sharma et al., 2007). The range of SW:HF mixtures were reacted, resulting in the overall effect of precipitating Fe-bearing sulfide and oxide minerals and anhydrite at a range of conditions representative of mixing in the subseafloor of MOR hydrothermal environments. Additional simulations representing SW:HF mixing at chemical conditions representative of ultramafic-hosted MOR hydrothermal systems are shown in the supplementary information (Figs. S1 and S2).

2.6 Os Partitioning Model Parameters between Pyrite and Hydrothermal Fluid

The output of the thermodynamic SW:HF mixing simulations was coupled with the experimentally determined $D_{Os/Fe}^{Pyrite}$ between pyrite and hydrothermal fluid to model the change in dissolved Os concentration within the hydrothermal fluid upon pyrite precipitation in the subseafloor through the Rayleigh distillation equation (Elderfield et al., 1996), as follows:

$$\left(\frac{[\mathrm{Os}]_{\mathrm{Fluid}}}{[\mathrm{Fe}]_{\mathrm{Fluid}}}\right) = \left(\frac{[\mathrm{Os}]_{\mathrm{Initial}}}{[\mathrm{Fe}]_{\mathrm{Initial}}}\right) \bullet f^{\left(D_{Os/Fe}^{Pyrite} - 1\right)} \qquad (5)$$

The change in the concentration of dissolved Os upon pyrite precipitation, $[Os]_{Fluid}$, is a function of $D_{Os/Fe}^{Pyrite}$, the degree of dissolved Fe remaining from sulfide precipitation, *f*, and the initial Os concentration, $[Os]_{Initial}$, prescribed to be between 10^2-10^4 fmol/kg, for pristine high temperature fluid within the subseafloor of the Main Endeavour and Axial Volcano hydrothermal systems along the Juan de Fuca Ridge (*i.e.* fluid that had not yet been mixed with conductively heated seawater). The $[Os]_{Initial}$ was estimated through dissolved Os mixing relationships between sampled hydrothermal fluid and seawater and independently through the assumption that Os and Sr are removed from basalts during hydrothermal alteration in similar proportions by Sharma et al. (2000) and Sharma et al. (2007), respectively. The initial dissolved Fe concentration, $[Fe]_{Initial}$, was prescribed to be 4 mmol/kg, similar to the concentration utilized for the GWB SW:HF mixing simulations. The SW:HF mixing simulations provide the dissolved Fe concentration throughout reaction progress, $[Fe]_{Fluid}$, and the fractional amount of remaining dissolved Fe, *f*:

$$f = \frac{[Fe]_{Fluid}}{[Fe]_{Initial}} \quad (6)$$

The concept of Rayleigh partitioning to describe the mass transfer of Os in dynamic systems, such as in the subseafloor, is appropriate due to the rapid precipitation and limited amount of exchange with the rapidly ascending hydrothermal fluid from the deep reaction zone. This is justified by previous pyrite precipitation experiments, which showed that pyrite does not exchange significantly with hydrothermal fluid at 350°C, especially throughout the course of this specific experiment, < 300 hours (Syverson et al., 2013; Syverson et al., 2015).

Together, the geochemical SW:HF mixing calculations, Rayleigh partitioning, and mass balance relations simulate the degree of sulfide precipitation upon mixing of conductively-heated seawater with high temperature end-member hydrothermal fluid. Collectively, this provides an estimate on the degree of removal of hydrothermally derived-Os into pyrite, and sulfide minerals more generally, in the subseafloor and the potential of unradiogenic Os contributing to the oceanic mass balance from MOR hydrothermal systems to seawater.

3. Results

3.1 Experimental Chemistry of Fluid and Pyrite

The effect of trace and major element contribution to the blank experimental reactant solution was examined at pH and Cl^- concentration conditions similar to the pyrite precipitation experiment. The results of the blank experiment demonstrate that the contribution of Fe and Os to the hydrothermal reactant fluid amounted to be 0.43 mmol/kg and 1.4 pmol/kg, respectively (Table 1). The initial dissolved concentrations of Fe and Os from the pyrite precipitation experiment were approximately 39 mmol/kg and 2 μmol/kg, respectively (Fig. 2a and Table 1). Upon the addition of the thiosulfate solution into the reactor and disproportionation to dissolved H_2S and HSO_4^-, the concentration of dissolved Fe and Os decreased markedly, to approximately 13 mmol/kg and 67 pmol/kg, respectively, as a result of pyrite precipitation and incorporation of Os within the formed precipitate (Fig. 2b). With increasing degrees of reaction progress, Fe and Os decreased in concentration until reaching a near steady-state composition, approximately 13 mmol/kg and 4 pmol/kg, respectively, over the course of approximately 300 hours. The dissolved S-species remained at a near steady state concentration of approximately 14 and 68 mmol/kg for H_2S and

HSO_4^-, respectively. The calculated $D^{Os/Fe}_{Pyrite-Fluid}$, as determined through Equation 5, ranged from approximately 10 and 15 throughout the experiment, with an average of 13.

Scanning electron microscopy images of the product pyrite recovered at the termination of the experiment demonstrate that pyrite is the sole sulfide product formed. The morphology of the pyrite precipitate is euhedral with a grain size distribution ranging from submicron to a few tens of microns in length, similar to pyrite precipitate formed from experiments conducted by Syverson et al. (2013) and Syverson et al. (2015) (Fig. 2b). The resulting Raman spectrum demonstrated that the mineral formed during the experiment was pyrite (Fig. S3), with diagnostic peaks at 340, 375, and 433 cm^{-1}, consistent with pyrite spectra in the RRUFF database (Downs, 2006) as well as those presented by White (2009). Further, BSE images of the polished grain mounts of the pyrite precipitate and analysis via EDS corroborate that pyrite is the sole sulfide mineral formed in Expt. #1 (Figs. S4 and S5).

Thermodynamic modeling of the overall solution chemistry indicates that pyrite is undersaturated with respect to the fluid composition, similar to fluid saturation calculations from pyrite precipitation experiments performed at the same physiochemical conditions by Syverson et al. (2013) and Syverson et al. (2015). The calculated undersaturation of pyrite is likely attributed to the inability of the HKF equation state to properly describe the molecular-scale contributions to the fluid dynamics at the prescribed experimental conditions (Driesner, 2013; Scheuermann et al., 2019). The calculated *in-situ* pH at experimental conditions is determined to be 2.7. The speciated log activities of H_2 and H_2S, as determined from total dissolved concentrations of H_2S and SO_4^{2-}, result in an average of -5.53 and -1.92, respectively, or in terms of log fugacity $O_2(g)$ and $S_2(g)$, -

24.97 and -4.35, respectively. Comparison of the speciated solution chemistry with respect to the Os-bearing mineral stability fields indicates that OsS_2 is expected to be stable at experimental conditions (Fig. 2c). Speciation calculations of dissolved Fe were used as an analogue for the speciation of dissolved Os (Fig. S6). The Fe-Cl speciation results at the representative pH values of the experiments, $pH_{350°C}$ of 2.7, versus MOR fluids, $pH_{350°C}$ approximately between 4.5 and 5.0, indicate negligible differences in the overall speciation of dissolved Fe, thus, likely the same for dissolved Os. Overall, these results indicate that the Os/Fe partition coefficient between pyrite and fluid determined in this experimental study is valid for the interpretation of Os-partitioning during sulfide mineralization at physiochemical conditions representative of MOR hydrothermal environments.

Comparison of the observed changes in the dissolved Os concentration before and after the precipitation event relative to the measured Os concentration of pyrite allowed quantification of the integrity of mass balance within the experimental system and the homogeneity of Os in pyrite. Triplicate analysis of the Os concentration in the product pyrite demonstrated slight Os heterogeneity in product pyrite with an average of 183 ± 11 ppm with a range of approximately 22 ppm. In consideration of the Os heterogeneity in product pyrite, the overall Os mass balance indicates that approximately 86-96 % of Os is accounted for within the entirety of the experimental system, primarily retained in product pyrite relative to residual dissolved Os. This confirms that Os is not lost within the experimental reactor and during the sampling, purification, and loading procedures required for N-TIMS analysis. Further, the $^{187}Os/^{188}Os$ ratios of the experimental solutions and pyrite are similar to the DROsS composition used to enrich the reactant solution with

dissolved Os, suggesting negligible Os contamination throughout the experiment and isotope fractionation upon partitioning into pyrite precipitate.

3.2 Os Concentration and Isotope Composition of EPR 9°50'N Sulfide

The Os concentration and $^{187}Os/^{188}Os$ isotope composition of the chalcopyrite sampled from the chimney sulfide recovered from the P-vent at the EPR 9°50'N hydrothermal system is 4.46 ppt and 0.2096, respectively (Figs. 1 and 3, Table 1). The Os concentration and isotopic composition of this chalcopyrite separate is similar to chimney sulfide sampled from the EPR 21°N hydrothermal system and is similar in Os isotopic composition of the sampled hydrothermal fluids sampled from the Juan de Fuca Ridge hydrothermal systems, Axial Volcano and Main Endeavour (Roy-Barman and Allègre, 1994; Sharma et al., 2000; Sharma et al., 2000).

3.3 Os/Fe Mixing and Pyrite-Fluid Partitioning Modeling

The SW:HF mixing calculations were simulated between the mass ratios of 0 and 4 (Fig. 4). The simulations indicate significant changes in fluid chemistry and minerals formed throughout this SW:HF mixing range. For example, upon increasing SW:HF mass mixing ratios of conductively heated seawater (250°C) with high temperature hydrothermal fluid (400°C), the fluid mixture temperature decreased from 400°C to approximately 280°C (Fig. 4a). Additionally, dissolved Fe^{2+} decreased significantly as a result of the precipitation of Fe-bearing sulfide minerals, predominantly pyrite, and the pH evolved to more acidic conditions to maintain charge balance upon mineral formation (Figs. 4b-d).

For the Os modeling calculations (Fig. 5), the relative change in dissolved Fe, *f*, (Figs. 4b and 5a) is used to model the change in the Os concentration (Fig. 5b). This effectively accounts for the change in the Os concentration of hydrothermal fluid upon partitioning with sulfide-mineral precipitate (Equation 5), where the change in the SW:HF mixing ratio is the primary control dictating the amount of sulfide formed, i.e. the change in *f* (Equation 6). Knowledge of the change in the unradiogenic Os concentration of the hydrothermal fluid upon mixing with seawater, with a known Os concentration of approximately 50 fmol/kg and $^{187}Os/^{188}Os$ ratio of 1.06, can then be used to predict the change in the $^{187}Os/^{188}Os$ composition upon sulfide precipitation during SW:HF mixing, where pristine hydrothermal fluid is predicted to have an $^{187}Os/^{188}Os$ composition of approximately 0.126 (Fig. 5c) (Sharma et al., 2007; Sharma et al., 2000). The change in the Os concentration and isotope composition are coupled through the degree of dissolved Fe^{2+} removed, *f*, upon SW:HF mixing, and are modeled together for comparison with natural hydrothermal fluids and sulfide minerals (Fig. 6).

4. Discussion

4.1 Mineral and Fluid Speciation and Solubility of Os at Hydrothermal Conditions

As previously reported, the expected speciation of dissolved Os at experiment conditions is likely complexed to chloride in the form of distorted octahedral Cl-complexes, such as $[OsCl_x(H_2O)_{6-x}]_{2-x}$, where x = 0-2 (Brugger et al., 2016; Xiong and Wood, 2000). Experimental results in this study indicate dissolved Os concentrations approximately 10^2-10^3 times less in magnitude relative to solubility measurements of pure OsS_2 and OsO_2 in saline solutions at elevated temperatures, 400 – 500 °C (Xiong and Wood, 2000). This observation suggests that the Os/Fe solid solution within pyrite is controlling the solubility of dissolved Os in the reactor solution rather than a distinct Os-

mineral (Xiong and Wood, 2000). Additionally, the time-series change in the concentration of both dissolved Os and Fe upon pyrite formation suggests that the elements co-precipitated as pyrite. Further, solid characterization through SEM imaging, Raman spectroscopic measurements, and EDS (Fig. 2b, S3 – S5) collectively corroborate that pyrite was the sole mineral formed, where Os exists as a trace element within pyrite.

4.2 MOR High Temperature Hydrothermal Fluids

Together, the experimental results and geochemical modeling validate the hypothesis that the process of pyrite precipitation in the subseafloor of MOR hydrothermal systems acts as a significant control on the concentration and isotope composition of Os in deep-seated hydrothermal fluids (Figs. 2 – 6). For example, Sharma et al. (2000) and Sharma et al. (2007) calculated, through conservative mixing relationships, the original Os isotopic composition and concentration of natural high temperature hydrothermal fluids prior to significant sulfide precipitation in the subseafloor. Specifically, for the Main Endeavour and Axial hydrothermal systems, the aforementioned authors utilized mass balance modeling of Os and Sr concentration and isotope composition of sampled hydrothermal fluids and seawater to calculate the composition of pristine deep-seated fluids in the subseafloor. Their calculations result in enriched Os concentrations for pristine hydrothermal fluids, approximately between 1300-2600 fmol/kg, significantly greater than the concentration of Os in seawater, which is approximately 50 fmol/kg. The predicted elevated Os concentration of these pristine endmember hydrothermal fluids is largely different from sampled high temperature vent fluids emanating from the seafloor, which have Os concentrations that are significantly depleted, approximately between 10 and 200 fmol/kg, and have $^{187}Os/^{188}Os$ compositions intermediate between MORB and seawater (Figs. 3 and 6a).

This comparison provides insight on the controls dictating the concentration of Os and its isotopes of sampled high temperature fluids which indicate a contribution of circulating conductively heated seawater mixing with hydrothermal fluid, effectively inducing significant precipitation of pyrite in the subseafloor and chemical modification of the buoyantly rising hydrothermal fluid. Specifically, the model results relative to the Os concentration and isotopic composition of fluids sampled from the Juan de Fuca Ridge (JdFR) hydrothermal systems indicate that approximately 10-15% of dissolved Fe is removed as sulfide precipitate within the subseafloor (Fig. 6c).

No other high temperature hydrothermal fluids have been sampled from active MOR environments specifically for Os concentration and $^{187}Os/^{188}Os$ analysis. Other estimates have been made by the utilization of Os concentration and isotope systematics of sulfide minerals and metalliferous sediments to predict the Os composition of hydrothermal fluids from which they are formed upon mixing with seawater (Brügmann et al., 1998; Cave et al., 2003) (Fig. 6a). Specifically for the basalt-hosted TAG hydrothermal system, Brügmann et al. (1998) estimated the hydrothermal fluid composition from the Os composition of massive sulfides sampled from the interior of an active sulfide mound, resulting in an Os concentration and $^{187}Os/^{188}Os$ composition of approximately 160 fmol/kg and 0.37, respectively. This predicted Os composition of hydrothermal fluid from TAG is similar to the fluids sampled from the basalt-hosted JdFR hydrothermal systems. Together, the basalt-hosted high temperature hydrothermal fluids have an average Os concentration and $^{187}Os/^{188}Os$ composition of 70 fmol/kg and 0.24, respectively. Alternatively, elevated Os concentration and the intermediate $^{187}Os/^{188}Os$ isotopic composition of metalliferous sediment surrounding the ultramafic-hosted Rainbow hydrothermal system along the Mid-Atlantic Ridge have collectively been used to predict the Os concentration of high temperature hydrothermal fluid

venting from the seafloor into the overlying seawater column (Cave et al., 2003). In particular, this study predicts high concentrations of unradiogenic Os, approximately between 500 and 1400 fmol/kg, in hydrothermal fluids venting from the seafloor at Rainbow, much greater in concentration relative to measured concentration Os of vent fluids from the JdFR basalt hosted hydrothermal systems. This comparison suggests that the pristine deep-seated hydrothermal fluid in the subseafloor of ultramafic-hosted systems, such as Rainbow, must also be significantly greater in concentration than 500-1400 fmol/kg to account for sulfide precipitation effects in the subseafloor, possibly exceeding concentrations of 10 pmol/kg; as estimated through the Os concentration of primitive mantle and oceanic crust with a range of representative of water/rock ratios representative of reaction conditions in the subseafloor of MOR hydrothermal systems (Coogan and Dosso, 2012; Day, 2013; Peucker-Ehrenbrink et al., 2012).

4.3 MOR Sulfide Minerals

The modeled Os composition of MOR hydrothermal pyrite precipitate can be determined and compared with natural sulfide minerals sampled from a range of MOR hydrothermal systems (Figs. 3, 6b and 6c) (Brügmann et al., 1998; Ravizza et al., 1996; Roy-Barman and Allègre, 1994; Zeng et al., 2014). The Os/Fe partitioning behavior of pyrite – fluid is expected to be similar to other sulfide minerals sampled from MOR hydrothermal systems (Fig. S7). For example, the median Os concentration of chimney-derived chalcopyrite is 23 ppt whereas chimney-derived pyrite is 17 ppt. The dataset suggests that both chalcopyrite and pyrite have a similar affinity for partitioning Os derived from hydrothermal fluid. In general, the Os concentration and $^{187}Os/^{188}Os$ composition of sulfide minerals vary significantly depending on the sampling site within hydrothermal environments located throughout a range of MOR spreading centers. The dredged

chimney and massive sulfides presented by Zeng et al. (2014) are sampled from a range of MOR environments from ultramafic-hosted to basalt-hosted hydrothermal systems, where the former is expected to be relatively enriched in PGE (Kuhn et al., 2005). However, comparison of the Os concentration of the massive sulfides sampled from this particular dataset demonstrate no clear Os concentration difference but are suggestive of forming from Os-bearing hydrothermal fluids at concentrations similar to or greater than 10^3 – 10^4 fmol/kg. The $^{187}Os/^{188}Os$ composition of these dredged chimney and massive sulfides, however, exhibit signatures indicative of post-depositional processes. These processes could include interaction with circulating seawater in the subseafloor, such as during sulfide recrystallization and mass-reworking of massive sulfides, as well as low-temperature oxidization of extinct hydrothermal sulfide deposits. For example, the near seawater $^{187}Os/^{188}Os$ signature but elevated Os concentration of these particular massive sulfides suggest that unradiogenic Os is either lost to seawater and effectively replaced by seawater-derived Os, and/or, the original $^{187}Os/^{188}Os$ composition of the sulfide minerals becomes significantly modified due to strong scavenging and enrichment of seawater-derived radiogenic Os onto secondary sulfide- and Fe-oxide minerals formed in the subseafloor and at the seafloor-seawater interface (Figs. 3, 6b, 6c, and 8). These processes may contribute to the wide range in $^{187}Os/^{188}Os$ compositions of dredged chimney sulfide separates from the TAG hydrothermal system presented by Ravizza et al. (1996), which also span the entire range between MORB and seawater, but are at elevated concentrations, approximately between 10^4 and 10^7 fmol/kg, similar to what is expected for sulfide minerals formed within active sulfide chimneys from relatively pristine hydrothermal fluids (Figs. 3, 6b and 6c).

Distinct differences exist in the range of Os concentration and $^{187}Os/^{188}Os$ isotopic composition between sulfide mineral samples taken from active hydrothermal environments, such as for the TAG massive pyrite sampled from the subseafloor of the actively forming sulfide mound, relative to chimney sulfide minerals sampled from the interior of active vents at the EPR 9°50'N and 21°N (Fig. 3 and Fig. 6b and c) (Brügmann et al., 1998; Roy-Barman and Allègre, 1994). The TAG and EPR hydrothermal systems are basalt hosted along slow and fast-spreading MOR centers, respectively. The massive pyrite range in Os concentration approximately between 10^2 to 10^4 fmol/kg and have an intermediate $^{187}Os/^{188}Os$ range between seawater and MORB, with an average of $^{187}Os/^{188}Os$ ratio of 0.95 (Brügmann et al., 1998). The distribution in Os concentration and isotopic composition of the TAG massive pyrite compared to the modeled pyrite composition indicate that the pyrite formed from a highly modified hydrothermal fluid that had a significant fraction of dissolved Fe removed upon pyrite precipitation in the subseafloor, approximately 30 % (Fig. 6c). Comparatively, chalcopyrite sampled from the interior of active sulfide chimneys, such as from the EPR 9°50'N (Fig. 1, ALV 5009) and from the EPR 21°N hydrothermal system (ALV 981) (Figs. 3, 6b and 6c), indicate that the minerals form from the mixing of hydrothermal fluids that are predominantly unradiogenic and elevated in concentration, up to 1000 fmol/kg, with a small contribution of admixed seawater (Roy-Barman and Allègre, 1994). Specifically, the chalcopyrite samples from EPR 9°50'N and 21°N have Os concentrations and $^{187}Os/^{188}Os$ compositions ranging approximately between $2\text{-}6\times10^4$ fmol/kg and 0.2096 and 0.2515, respectively. The chalcopyrite sulfide separates are in close agreement with modeling predictions for a fraction of approximately 85-90 % of dissolved Fe^{2+} remaining in the hydrothermal fluid, similarly predicted from the composition of high temperature fluids sampled from chimney

structures at the basalt-hosted MEF and Axial Volcano hydrothermal systems along the JdFR (Fig. 6c).

Disregarding samples representative of $^{187}Os/^{188}Os$ post-depositional effects, the compositional differences between the massive sulfide minerals relative to chimney sulfide minerals likely reflect significant differences in the hydrothermal flow pathway in the subseafloor. Specifically, high temperature hydrothermal fluids may be focused along conduits from the deep-seated reaction zone to the seafloor, allowing significant unradiogenic Os transport to the seawater with limited sulfide precipitation. In contrast, diffuse fluids may mix with progressive amounts of conductively-heated seawater circulating in the subseafloor, generating massive sulfides from SW:HF fluid mixtures with very little dissolved unradiogenic Os remaining with an $^{187}Os/^{188}Os$ signature of the SW:HF fluid mixture similar to the composition of seawater.

4.4 MOR Os Contribution to the Oceanic Mass Balance

The flux estimated in this study may underestimate the contribution from ultramafic-hosted high temperature MOR hydrothermal systems, which may account for up to ~30 % of all hydrothermal systems and are predicted to produce high-temperature fluids with Os concentrations significantly greater than basalt-hosted systems (Figs. 3 and 6a) (Coogan and Dosso, 2012; Sharma et al., 2007; Sharma et al., 2000). For example, the modern flux of Os into seawater sourced from high temperature basaltic-hosted MOR hydrothermal systems is estimated from this study to be 0.7 – 4.2 mol/yr, as determined from the average hydrothermal Os concentration of fluids from the basaltic systems, and range of the hydrothermal H_2O flux, 70 fmol/kg and 1×10^{13} – 6×10^{13} kg H_2O/yr, respectively, with a $^{187}Os/^{188}Os$ range skewed towards the composition of unradiogenic

oceanic crust (Fig. 3) (Brügmann et al., 1998; Elderfield and Schultz, 1996; Sharma et al., 2007; Sharma et al., 2000). Depending on the hydrothermal fluid flux, this high-temperature MOR Os flux is similar and encapsulates previous estimates reported by Sharma et al. (2000) and Sharma et al. (2007) (2.8 mol/yr). This value is significantly smaller than the hydrothermal Os flux used by Li and Elderfield (2013) (52 mol/yr), suggesting there still may be a missing source of unradiogenic Os and thus an imbalance in the modern Os mass balance. As also suggested by Sharma et al. (2007) and Peucker-Ehrenbrink and Ravizza (2000), the deficit in a source of unradiogenic Os to the oceans may be attributed to the fact that basalt hosted systems have only been investigated and other Os sources, such as low temperature weathering of oceanic crust, remain largely unconstrained (Sharma et al., 2007).

The transition in the physiochemical conditions experienced by the hydrothermal fluid upon venting into cold and oxidizing seawater induces significant changes in the speciation of dissolved Os and will have an effect on the fate of hydrothermally-derived Os in seawater. For example, in high-temperature hydrothermal fluids at subseafloor MOR physiochemical conditions, dissolved Os is predicted to exist as Os^{2+} and complexed with dissolved Cl^- (Xiong and Wood, 2000). Upon venting into oxidizing seawater, hydrothermally derived dissolved Os is expected to become oxidized and exist predominantly as an oxyanion species, similar to dissolved V and Mo in modern seawater, and may complex to dissolved organic ligands and become scavenged onto Fe^{3+}-oxide minerals and/or organic matter within the hydrothermal plume overlying the seafloor hydrothermal system (Cave et al., 2003; Palmer et al., 1988; Ravizza et al., 2001a; Ravizza and McMurtry, 1993; Woodhouse et al., 1999). On a much broader scale, changes in atmospheric and seawater chemistry throughout Earth's past may have influenced the physiochemical processes within high-

temperature hydrothermal systems and thus the amount of sulfide precipitation in the subseafloor, which could potentially alter the hydrothermal Os flux (Antonelli et al., 2017; Kump and Seyfried, 2005). It is clear that uncertainties in the Os system still exist, and future studies are encouraged. Nevertheless, our results corroborate the efficient control of sulfide mineral precipitation on the source of hydrothermal Os, indicating that, in the modern environment, the flux of unradiogenic hydrothermal Os plays a minimal role in the Os oceanic mass balance (Peucker-Ehrenbrink et al., 2003; Peucker-Ehrenbrink et al., 2012; Peucker-Ehrenbrink and Ravizza, 2000; Ravizza et al., 1996; Sharma et al., 2007; Sharma et al., 2000).

5. Conclusions

Experimental and geochemical results from this study demonstrate that dissolved Os derived from deep-seated hydrothermal systems along the MOR system is strongly affected by partitioning into sulfides, such as pyrite, upon precipitation within the subseafloor. Natural sulfides from active and inactive MOR hydrothermal environments corroborate the inference that fluids are enriched in dissolved Os at concentrations greater than 1000 fmol/kg, prior to sulfide precipitation. This study highlights the need to perform more experimental studies which focus on the partitioning systematics of trace and ultra-trace elements between minerals and fluid, that are increasingly used as geochemical proxies to better understand Earth system processes. Conditions, which are not considered magmatic, but at hydrothermal and low temperature conditions, are subjected to PGE partitioning effects and should be further examined to elucidate the processes imposing these signatures recorded in minerals and fluids. Using similar novel experiments and characterization techniques, such as EXAFS synchrotron measurements, will expand our understanding of the coordination and oxidation state of Os and PGE within fluids and minerals in complex

hydrothermal environments. The coupling of experiments with thermodynamic modeling is a powerful tool as it provides a process-oriented perspective on how mineral formation dictates the fate of highly siderophile and chalcophile elements at a range of physiochemical conditions representative of hydrothermal environments.

Acknowledgements

The paper benefited from constructive comments and recommendations of the anonymous reviewer, Dr. Tatsuo Nozaki, and GCA-AE, Dr. Jun-Ichiro Ishibashi. This study was funded primarily through the Flint Postdoctoral Fellowship awarded to DDS. DDS conducted the experiments and wrote the majority of the manuscript with the assistance of JK. LRY wrote the GWB script to allow for complex simulation of fluid mixing. BMT compiled Os thermodynamic data into an internally consistent thermodynamic database and coordinated mineralogical characterization of pyrite precipitates. WES provided the experimental equipment necessary for this study and acknowledges support from a National Science Foundation (NSF) grant (NSF-OCE-1736670). LRY was funded by the NSF Postdoctoral Research Fellowship in Biology (NSF-DBI-1812035). ADR performed the Os concentration and isotopic measurements of the experimental solutions, product pyrite, and the natural sulfide presented in this study. DDS would like to thank Dr. Dionysis Foustoukos (Carnegie Institute of Science) for sharing knowledge on experimental studies focused on Os. DDS also thanks Dr. Changle Wang and Cerys Holstege (Yale University) for providing assistance on the processing of samples and concentration measurements by ICP-MS. Finally, DDS would like to thank NSF and WHOI, the crew, the ECS team, ECS mentors, Drs. Dan Fornari (WHOI) and Mike Perfit (University of Florida), co-chiefs of the ECS cruise, Drs. Elizabeth Trembath-Reichert (Arizona State University) and Ross Parnell-Turner (Scripps

Institute of Oceanography), and the NDSF HOV *Alvin* and AUV *Sentry* scientific teams aboard the R/V *Atlantis* on the AT42-06 expedition to the EPR 9°50'N hydrothermal system (NSF-OCE-1834797). Simone Pujatti and Robert Marr (both UCalgary) are thanked for their assistance with Raman spectroscopy and EMP/EDS analyses, respectively. Copyright for the image of P-vent (Fig. 1a) is by WHOI 2018, NDSF, *Alvin* Group, and NSF.

Figure Captions

Fig. 1: Digital images of the high temperature P-vent sulfide structure emitting black smoker fluid (355°C) from the EPR 9°50'N, and the lengthwise- and cross-section of the P-vent chimney structure that was sampled to extract sulfide mineral from the chimney interior for Os concentration and isotopic analysis, a-c, respectively.

Fig. 2: a) The experimental change in dissolved Fe and Os as a consequence of pyrite formation. The uncertainty associated with the Fe and Os measurements are smaller than the gray and blue symbols, respectively. b) Scanning electron microscopy image of the product pyrite recovered at the termination of Expt. #1. c) Stability diagram of Os-bearing minerals relative to the speciated experimental solution samples, indicating that the experimental system is within the stability field of OsS_2. Further, the geochemical model output of the SW:HF mass mixing simulations at chemical conditions representative of basalt-hosted MOR hydrothermal systems is shown by the gray region of Fig. 2c.

Fig. 3: Boxplots representing the Os concentration (a) and isotopic composition (b) distribution of each Os-bearing material sampled from MOR hydrothermal systems. The Os data of dredged sulfide minerals are derived from a large range of MOR hydrothermal systems (Ravizza et al.,

1996; Zeng et al., 2014), active massive sulfide minerals are from core recovered during the ODP Leg 158 at the TAG hydrothermal system (Brügmann et al., 1998), hydrothermal fluids are from the Juan de Fuca Ridge (JdFR), Axial Volcano and Main Endeavour hydrothermal systems (Sharma et al., 2007; Sharma et al., 2000), and chimney sulfide minerals are sampled from active vents at the EPR 9°50'N and 21°N hydrothermal systems (this study and Roy-Barman and Allègre (1994), respectively). The $^{187}Os/^{188}Os$ of the sulfide minerals are predominantly bounded by the Os isotope compositions of seawater and oceanic crust, approximately 1.06 and 0.126, respectively. The Os concentrations for MORB and primitive mantle/peridotite are from Gannoun et al. (2007) and Day (2013). See Fig. S7 for sulfide mineral-specific Os concentration distributions between chalcopyrite, pyrite, sphalerite, pyrrhotite and massive pyrite.

Fig. 4: Thermodynamic calculations simulating the effect of seawater-hydrothermal fluid mass mixing ratios, SW:HF, at a range between 0 and 4. a) The change in temperature as a result of mixing conductively heated seawater at 250°C and hydrothermal fluid at 400°C. b and c) The change in dissolved Fe due to the formation of Fe-bearing minerals, primarily pyrite, and anhydrite. d) The change in pH reflecting proton production upon mineral precipitation.

Fig. 5: The model output from the SW:HF mixing simulations coupled with Os partitioning and isotope mass balance as a function of dissolved Fe removal due to sulfide precipitation. a) The degree of dissolved Fe^{2+} remaining in the hydrothermal fluid, *f*, as a function of SW:HF mixing ratios; b) the degree of dissolved Os removed and c) the change in $^{187}Os/^{188}Os$ of pristine hydrothermal fluid as a function of *f*, b and c, respectively. For Fig. 5b, the concentration values represent the initial Os concentration. Specifically, for Fig. 5b and 5c, the Os/Fe apparent partition

coefficient used for modeling is 13. For Fig. 5c, the $^{187}Os/^{188}Os$ ratio of the hydrothermal fluid is bracketed between the compositions of seawater and oceanic crust, as shown by the dashed lines.

Fig. 6: Model constraints on the Os concentration and $^{187}Os/^{188}Os$ composition during sulfide precipitation relative to natural observations of MOR hydrothermal fluids and sulfide minerals, which include chalcopyrite, pyrite, sphalerite, and pyrrhotite. a) Model comparison with Os observations of high temperature hydrothermal fluid sampled along the JdFR are shown in blue circle symbols. The predicted dissolved Os concentration and $^{187}Os/^{188}Os$ composition of fluids from TAG and Rainbow are shown in green and white circle symbols, respectively (Brügmann et al., 1998; Cave et al., 2003). b) Comparison of hydrothermal sulfide minerals from a range of MOR vent systems with the model Os concentration and $^{187}Os/^{188}Os$ composition relations (Brügmann et al., 1998; Ravizza et al., 1996; Roy-Barman and Allègre, 1994; Zeng et al., 2014). c) The distribution and median of sampled hydrothermal fluids, active massive sulfides and chimney sulfides, and dredged sulfides, which are described as the blue circle, green triangle and purple pentagon, and orange square, respectively. The horizontal tie lines indicate the relative amount of dissolved Fe^{2+} remaining in the modeled hydrothermal fluid. The plot symbols and colored areas are representative of the legend symbols in Figs. 6a and 6b for fluid and minerals, respectively. Also, it is reminded that multiple sulfide minerals were plotted in comparison with the Os/Fe partition model, specifically chalcopyrite, pyrite, sphalerite, pyrrhotite, and massive pyrite (Fig. S7).

Table 1: Time-series sampled fluid chemistry of the pyrite precipitation experiment at 350˚C and [illegible] MPa.

[a]Sample	Time (hr)	Soln. Mass	$pH_{25°C}$	$[Fe^{2+}]$	$[Os^{2+}]$	$[H_2S]$	$[SO_4]$	$^{187}Os/^{188}Os$	±	$D_{(Os/Fe)}$
0-0	-	47.0	1.03	0.43	1.4	n.a.	n.a.	0.2306	0.05	-
1-0	-	43.6	1.02	39.20	2090130	n.a.	n.a.	0.1609	0.01	-
$Na_2S_2O_3$ inj.	0	*4.0	6.67	-	-	-	-	-		-
1-1	1	38.0	1.22	17.93	67.1	[illegible]	70	0.1609	0.01	13.23
1-2	32	34.0	1.25	17.65	[illegible]	16.2	68	0.1609	0.02	14.88
1-3	74	30.3	1.27	16.98	[illegible].4	n.a.	n.a.	0.1609	0.04	15.01
1-4	147	26.3	1.19	14.49	[illegible].8	n.a.	n.a.	0.1608	0.11	13.57
1-5	194	22.4	1.19	11.26	[illegible]7.1	12.9	65	0.1608	0.05	10.09
1-6	266	16.4	1.18	13.16	4.1	n.a.	n.a.	0.1608	0.09	12.05

Pyrite Product (g)	$[Os]_b$ (ppm, n=3)	$^{187}Os/^{188}Os$	±	Chalcopyrite [illegible]2.9°0'N	[Os] (ppt, n=1)	$^{187}Os/^{188}Os$	±	Average $D_{(Os/Fe)}$
0.10	183 ± 11	0.1608	0.01		4.46	0.2096	0.001	13.14

[a]The solution mass is reported in grams and all dissolved concentrations are represented in mmol/kg except for dissolved Os, which is in pmol/kg. Sample 0-0 is representative of the blank solution sampled at experimental conditions (i.e. no initial dissolved Fe and Os). The injection of the Na-thiosulfate solution, prior to sampling event 1-1, is indicated by the presence of sulfur species in the system. Time "zero" is immediately after the thiosulfate injection. *Amount (grams) of Na-thiosulfate solution injected into gold cell. The solution mass reported is representative of the mass before each sampling event.

References

Antonelli, M.A., Pester, N.J., Brown, S.T. and DePaolo, D.J. (2017) Effect of paleoseawater composition on hydrothermal exchange in midocean ridges. Proceedings of the National Academy of Sciences 114, 12413-12418.

Berndt, M.E., Seyfried, W.E. and Beck, J.W. (1988) Hydrothermal alteration processes at mid-ocean ridge: Experimental and theoretical constraints from Ca and Sr exchange reactions and Sr isotopic ratios. Journal of Geophysical Research 93, 4573-4583.

Bethke, C.M., Farrell, B. and Yeakel, S. (2018) The Geochemist's Workbench® Release 12.0 - Reaction Modeling Guide.

Birck, J.L., Roy-Barman, M. and Capmas, F. (1997) Re-Os Isotopic Measurements at the Femtomole Level in Natural Samples. Geostandards and Geoanalytical Research 21, 19-27.

Blount, C.W. and Dickson, F.W. (1969) The solubility of anhydrite ($CaSO_4$) in NaCl-H2O from 100 to 450C and 1 to 1000 bars. Geochimica et Cosmochimica Acta 33, 227-245.

Brandon, A.D., Creaser, R.A., Shirey, S.B. and Carlson, R.W. (1996) Osmium recycling in subduction zones. Science 272, 861-864.

Brenan, J.M., Bennett, N.R. and Zajacz, Z. (2016) Experimental Results on fractionation of the highly siderophile elements (HSE) at Variable Pressures and Temperatures during Planetary and Magmatic Differentiation. Reviews in Mineralogy and Geochemistry 81, 1-87.

Brugger, J., Liu, W., Etschmann, B., Mei, Y., Sherman, D. and Testemale, D. (2016) A review of the coordination chemistry of hydrothermal systems, or do coordination changes make ore deposits? Chemical Geology 447, 219-253.

Brügmann, G.E., Birck, J.L., Herzig, P.M. and Hofmann, A.W. (1998) Os isotopic composition and Os and Re distribution in the active mound of the TAG hydrothermal system, Mid-Atlantic Ridge. Proceedings of the Ocean Drilling Program, Scientfic Results 158, 91-99.

Carlson, R.W. (2005) Application of the Pt-Re-Os isotopic systems to mantle geochemistry and geochronology. Lithos 82, 249-272.

Cave, R.R., Ravizza, G., German, C., Thomson, J. and Nesbitt, R.W. (2003) Deposition of osmium and other platinum-group elements. beneath the ultramafic-hosted Rainbow hydrothermal plume. Earth and Planetary Science Letters 210, 65-79.

Cohen, A.S., Coe, A.L., Harding, S.M. and Schwark, L. (2004) Osmium isotope evidence for the regulation of atmospheric CO_2 by continental weathering. Geology 32, 157-160.

Cohen, A.S. and Waters, F.G. (1996) Separation of osmium from geological materials by solven extraction for analysis by thermal ionisation mass spectrometry. Analytica Chimica Acta 332, 269-275.

Coogan, L.A. and Dosso, S. (2012) An internally consistent, probalistic, determination of ridge-axis hydrothermal fluxes. Earth and Planetary Science Letters 323, 92-101.

Creaser, R.A., Papanastassiou, D.A. and Wasserburg, G.J. (1991) Negative thermal ion mass spectrometry of osmium, rhenium, and iridium. Geochimica et Cosmochimica Acta 55, 397-401.

Day, J.M.D. (2013) Hotspot volcanism and highly siderophile elements. Chemical Geology 341, 50-74.

Doerner, H.A. and Hoskins, W.M. (1925) Co-precipitation of radium and barium sulfates. Journal of the American Chemical Society 47, 662-675.

Downs, R.T. (2006) The RRUFF Project: an integrated study of the chemistry, crystallography, Raman and infrared spectroscopy of minerals. Program and Abstracts of the 19th General Meeting of the International Mineralogical Association in Kobe, Japan 117.

Driesner, T. (2013) The molecular-scale fundament of geothermal fluid thermodynamics. Reviews in Mineralogy and Geochemistry 76, 5-33.

Elderfield, H., Bertram, C.J. and Erez, J. (1996) A biomineralization model for the incorporation of trace elements into foraminiferal calcium carbonate. Earth and Planetary Science Letters 142, 409-423.

Elderfield, H. and Schultz, A. (1996) Mid-ocean ridge hydrothermal fluxes and the chemical composition of the ocean. Annu. Rev. Earth Planet. Sci. 24, 191-224.

Fleet, M.E., Crocket, J.H. and Stone, W.E. (1996) Partitioning of platinum-group elements (Os, Ir, Ru, Pt, Pd) and gold between sulfide liquid and basalt melt. Geochimica et Cosmochimica Acta 60, 2397-2412.

Foustoukos, D.I. (2019) Hydrothermal oxidation of Os. Geochimica et Cosmochimica Acta 255, 237-246.

Foustoukos, D.I., Bizimis, M., Frisby, C. and Shirey, S.B. (2015) Redox controls on Ni-Fe-PGE mineralization and Re/Os fractionation during serpentinization of abyssal peridotite. Geochimica et Cosmochimica Acta 150, 11-25.

Gannoun, A., Burton, K.W., Parkinson, I.J., Alard, O., Schiano, P. and Thomas, L.E. (2007) The scale and origin of the osmium isotope variations in mid-ocean ridge basalts. Earth and Planetary Science Letters 259, 541-556.

German, C. and Seyfried, W.E. (2014) Hydrothermal Processes, Treatise on Geochemistry, pp. 192-227.

Helgeson, H.C., Kirkham, D.H. and Flowers, G.C. (1981) Theoretical prediction of thermodynamic properties of aqueous electrolytes at high pressures and temperatures. IV. Calculation of activity coefficients, osmotic coefficients, and apparent molal and standard and relative partial molal properties to 600°C and 5kb. American Journal of Science 281, 1249-1516.

Knacke, O., Kubaschewski, O. and Hesselmann, K. (1991) Thermochemical properties of inorganic substances.

Kong, X.-Z., Tutolo, B.M. and Saar, M.O. (2013) DBCreate: A SUPCRT92-based program for producing EQ3/6, TOUGHREACT, and GWB thermodynamic databases at user-defined T and P. Computers & Geosciences 51, 415-417.

Kuhn, T., Brügmann, G.E., Petersen, S. and Herzig, P.M. (2005) Os isotopic ratios and PGE geochemistry in rocks and sulfides from the ultramafic-hosted Logatchev hydrothermal field, 14°45'N MAR. AGU Fall Meeting Abstracts.

Kump, L.R. and Seyfried, W.E. (2005) Hydrothermal Fe fluxes during the Precambrian: Effect of low oceanic sulfate concentrations and low hydrostatic pressure on the composition of black smokers. Earth and Planetary Science Letters 235, 654-662.

Li, G. and Elderfield, H. (2013) Evolution of carbon cycle over the past 100 million years. Geochimica et Cosmochimica Acta 103, 11-25.

Luguet, A., Nowell, G.M. and Pearson, D.G. (2008) 184Os/188Os and 186Os/188Os measurements by Negative Thermal Ionisation Mass Spectrometry (N-TIMS): Effects of intefering element and mass fractionation corrections on data accuracy and precision. Chemical Geology 248, 342-362.

Mills, R.A., Teagle, D.A.H. and Tivey, M.A. (1998) Fluid mixing and anhydrite precipitation within the TAG mound. Proceedings of the Ocean Drilling Program 158, 119-127.

Mills, R.A. and Tivey, M.K. (1999) Seawater entrainment and fluid evolution within the TAG hydrothermal mound: evidence from analyses of anhydrite. Mid-ocean ridges: dynamics of processes associated with creation of new ocean crust, 225-263.

Newton, R.C. and Manning, C.E. (2005) Solubility of Anhydrite, CaSO4, in NaCl-H2O Solutions at High Pressures and Temperatures: Applications to Fluid-Rock Interaction. Journal of Petrology 46, 701-716.

Nowell, G.M., Luguet, A., Pearson, D.G. and Horstwood, M.S.A. (2008) Precise and accurate 186Os/188Os and 187Os/188Os measurements by multi-collector plasma ionisation mass spectrometry (MC-ICP-MS) part I: Solution Analyses. Chemical Geology 248, 363-393.

Nozaki, T., Kato, Y. and Suzuki, K. (2013) Late Jurassic ocean anoxic event: evidence from voluminous sulphide deposition and preservation in the Panthalassa. Scientific Reports 3, 1-6.

Oxburgh, R., Pierson-Wickmann, A.C., Reisberg, L. and Hemming, S. (2007) Climate-correlated variations in seawater 187Os/188Os over the past 200,000 yr: Evidence from the Cariaco Basin, Venezuela. Earth and Planetary Science Letters 263, 246-258.

Palmer, M.R. (1992) Controls over the chloride concentration of submarine hydrothermal vent fluids: evidence from Sr/Ca and 87Sr/86Sr ratios. Earth and Planetary Science Letters 109, 37-46.

Palmer, M.R., Falkner, K.K., Turekian, K.K. and Calvert, S.E. (1988) Sources of osmium isotopes in manganese nodules. Geochimica et Cosmochimica Acta 52, 1197-1202.

Paquay, F. and Ravizza, G. (2012a) Heterogeneous seawater 187Os/188Os during the Late Pleistocene glaciations. Earth and Planetary Science Letters 349-350, 126-138.

Paquay, F.S. and Ravizza, G. (2012b) Heterogeneous seawater 187Os/188Os during the Late Pleistocene glaciations. Earth and Planetary Science Letters 349-350, 126-138.

Petersen, S., Herzig, P.M. and Hannington, M.D. (1998) Fluid inclusion studies as a guide to temperature regime within the TAG hydrothermal mound. Proceedings of the Ocean Drilling Program 158, 163-176.

Peucker-Ehrenbrink, B., Bach, W., Hart, S.R., Blusztajn, J.S. and Abbruzzese, T. (2003) Rhenium-osmium isotope systematics and platinum gropu element concentrations in oceanic crust DSDP/ODP Sites 504 and 417/418. Geochemistry Geophysics Geosystems 4, 1-28.

Peucker-Ehrenbrink, B., Hanghoj, K., Atwood, T. and Kelemen, P.B. (2012) Rhenium-osmium isotope systematics and platinum group element concentrations in oceanic crust. Geology 40, 199-202.

Peucker-Ehrenbrink, B. and Ravizza, G. (2000) The marine osmium isotope record. Terra Nova 12, 205-219.

Ravizza, G., Blusztajn, J.S. and Prichard, H.M. (2001a) Re-Os systematics and platinum-group element distribution in metalliferous sediments from the Troodos ophiolite. Earth and Planetary Science Letters 15, 369-381.

Ravizza, G., Martin, C.E., German, C.R. and Thompson, G. (1996) Os isotopes as tracers in seafloor hydrothermal systems: metalliferous deposits from the TAG hydrothermal area, 26°N Mid-Atlantic Ridge. Earth and Planetary Science Letters 138, 105-119.

Ravizza, G. and McMurtry, G.M. (1993) Osmium isotopic variation in metalliferous sediments from the East Pacific Rise and the Bauer Basin. Geochimica et Cosmochimica Acta 57, 4301-4310.

Ravizza, G., Norris, R.N., Blusztajn, J.S. and Aubry, M.P. (2001b) An osmium isotope excursion associated with the late Paleocene thermal maximum: Evidence of intensified chemical weathering. Paleoceanography 16, 155-163.

Rooney, A.D., Selby, D., Houzay, J.P. and Renne, P.R. (2010) Re-Os geochronology of a Mesoproterozoic sedimentary succession, Taoudeni basin, Mauritania: Implications for basin-wide correlations and Re-Os organic-rich sediments systematics. Earth and Planetary Science Letters 289, 486-496.

Rooney, A.D., Selby, D., Lloyd, J.M., Roberts, D.H., Luckge, A., Sageman, B.B. and Prouty, N.G. (2016) Tracking millenial-scale Holocene glacial advance and retreat using osmium isotopes: Insights from the Greenland ice sheet. Quaternary Science Reviews 138, 49-61.

Roy-Barman, M. and Allègre, C.J. (1994) 187Os/186Os ratios of mid-ocean ridge basalts and abyssal peridotites. Geochimica et Cosmochimica Acta 58, 5043-5054.

Scheuermann, P.P., Tutolo, B.M. and Seyfried, W.E. (2019) Anhydrite solubility in low-density hydrothermal fluids: Experimental measurements and thermodynamic calculations. Chemical Geology 542, 184-195.

Seewald, J.S. and Seyfried, W.E. (1990) The effect of temperature on metal mobility in subseafloor hydrothermal systems: constraints from basalt alteration experiments. Earth and Planetary Science Letters 101, 388-403.

Selby, D. and Creaser, R.A. (2004) Macroscale NTIMS and microscale LA-MC-ICP-MS Re-Os isotopic analysis of molybdenite: Testing spatial restrictions for reliable Re-Os age determinations, and implications for the decoupling of Re and Os within molybdenite. Geochimica et Cosmochimica Acta 68, 3897-3908.

Seyfried, W.E. and Ding, K. (1993) The effect of redox on the relative solubilities of copper and iron in Cl-bearing aqueous fluids at elevated temperatures and pressures: An experimental study with application to subseafloor hydrothermal systems. Geochimica et Cosmochimica Acta 57, 1905-1917.

Seyfried, W.E., Janecky, D.R. and Berndt, M.E. (1987) Rocking autoclaves for hydrothermal experiments: II. The flexible reaction-cell system. Hydrothermal Experimental Techniques, 216-239.

Seyfried, W.E., Pester, N.J., Ding, K. and Rough, M. (2011) Vent fluid chemistry of the Rainbow hydrothermal system (36°N, MAR): Phase equilibria and in situ pH controls on subseafloor alteration processes. Geochimica et Cosmochimica Acta 75, 1574-1593.

Sharma, M., Rosenberg, E.J. and Butterfield, D.A. (2007) Search for the proverbial mantle osmium sources to the oceans: Hydrothermal alteration of mid-ocean ridge basalt. Geochimica et Cosmochimica Acta 71, 4655-4667.

Sharma, M., Wasserburg, G.J., Hoffmann, A.W. and Butterfield, D.A. (2000) Osmium isotopes in hydrothermal fluids from the Juan de Fuca Ridge. Earth and Planetary Science Letters 179, 139-152.

Shikazono, H. and Holland, H.D. (1983) The partitioning of strontium between anhydrite and aqueous solution from 150 to 250C. Economic Geology Monographs 5, 320-328.

Shirey, S.B. and Walker, R.J. (1995) Carius tube digestion for low-blank rhenium-osmium analysis. Anal. Chem. 67, 2136-2141.

Shock, E.L., Helgeson, H.C. and Sverjensky, D.A. (1989) Calculation of the thermodynamic and transport properties of aqueous species at high pressures and temperatures: Standard partial molal properties of inorganic neutral species. Geochimica et Cosmochimica Acta 53, 2157-2183.

Shock, E.L., Oelkers, E.H., Johnson, J.W., Sverjensky, D.A. and Helgeson, H.C. (1992) Calculation of the thermodynamic properties of aqueous species at high pressures and temperatures: Effective electrostatic radii, dissociation constants, and standard partial molal properties to 1000°C and 5 kbar. Journal of the Chemical Society, Faraday Transactions 88, 803-826.

Shock, E.L., Sassani, D.C., Willis, M. and Sverjensky, D.A. (1997) Inorganic species in geologic fluids: Correlations among standard molal thermodynamic properties of aqueous ions and hydroxide complexes. Geochimica et Cosmochimica Acta 61, 907-950.

Stein, H.J., Markey, R.J., Morgan, J.W., Hannah, J.L. and Scherstén, A. (2001) The remarkable Re-Os chronometer in molybdenite: how and why it work. Terra Nova 13, 479-486.

Sun, R. and Ceder, G. (2011) Feasibility of band gap engineering of pyrite FeS2. Physical Review B 84, 1-7.

Sverjensky, D.A., Shock, E.L. and Helgeson, H.C. (1997) Prediction of the thermodynamic properties of aqueous metal complexes to 1000°C and 5 kbar. Geochimica et Cosmochimica Acta 61, 1359-1412.

Syverson, D.D., Borrok, D.M. and Seyfried, W.E. (2013) Experimental determination of equilibrium Fe isotopic fractionation between pyrite and dissolved Fe under hydrothermal conditions. Geochimica et Cosmochimica Acta 122, 170-183.

Syverson, D.D., Ono, S., Shanks, W.C. and Seyfried, W.E. (2015) Multiple sulfur isotope fractionation and mass transfer processes during pyrite precipitation and recrystallization: An experimental study at 300 and 350˚C. Geochimica et Cosmochimica Acta 165, 418-434.

Tanger, J.C. and Helgeson, H.C. (1988) Calculation of the thermodynamic and transport properties of aqueous species at high pressures and temperatures: Revised equations of state for the standard partial molal properties of ions and electrolytes. American Journal of Science 288, 19-98.

Teagle, D.A.H., Alt, J., Chiba, H. and Halliday, A.N. (1998) Dissecting an active hydrothermal deposit: The strontium and oxygen isotopic anatomy of the TAG hydrothermal mound-anhydrite. Proceedings of the Ocean Drilling Program 158, 129-141.

Tivey, M.K., Mills, R.A., and Teagle, D.A.H. (1998) Temperature and salinity of fluid inclusions in anhydrite as indicators of seawater entrainment and heating in the TAG active mound. Proceedings of the Ocean Drilling Program 158, 179-190.

Völkening, J., Walczyk, T. and Heumann, K.G. (1991) Osmium isotope ratio determinatinos by negative thermal ionization mass spectrometry. International Journal of Mass Spectrometry and Ion Processes 105, 147-159.

White, S.N. (2009) Laser Raman spectroscopy as a technique for identification of seafloor hydrothermal and cold seep minerals. Chemical Geology 259, 240-252.

Woodhouse, O.B., Ravizza, G., Kenison Falkner, K., Statham, P.J. and Peucker-Ehrenbrink, B. (1999) Osmium in seawater: vertical profiles of concentration and isotopic composition in the Easter Pacific Ocean. Earth and Planetary Science Letters 173, 223-233.

Xiong, Y. and Wood, S.A. (2000) Experimental quantification of hydrothermal solubility of platinum-group elements with special references to porphyry copper environments. Mineralogy and Petrology 68, 1-28.

Zeng, Z., Chen, S., Selby, D., Yin, X. and Wang, X. (2014) Rhenium-osmium abundance and isotopic compositions of massive sulphides from modern deep-sea hydrothermal systems:

Implications for vent associate ore forming processes. Earth and Planetary Science Letters 396, 223-234.

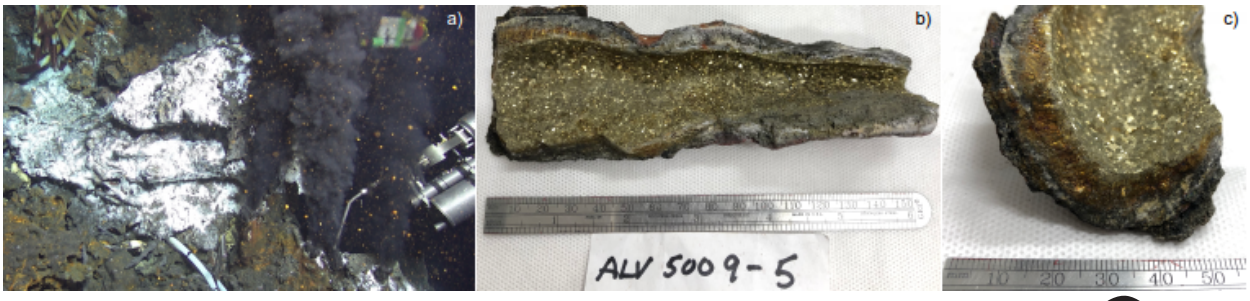

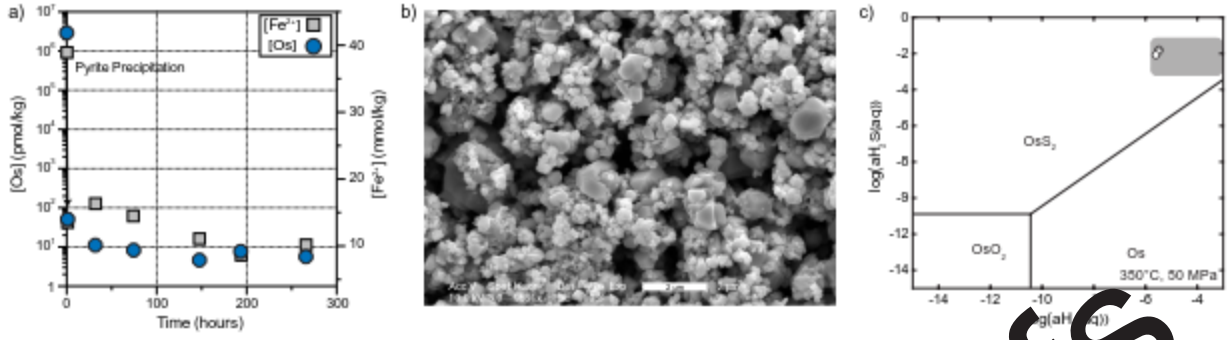

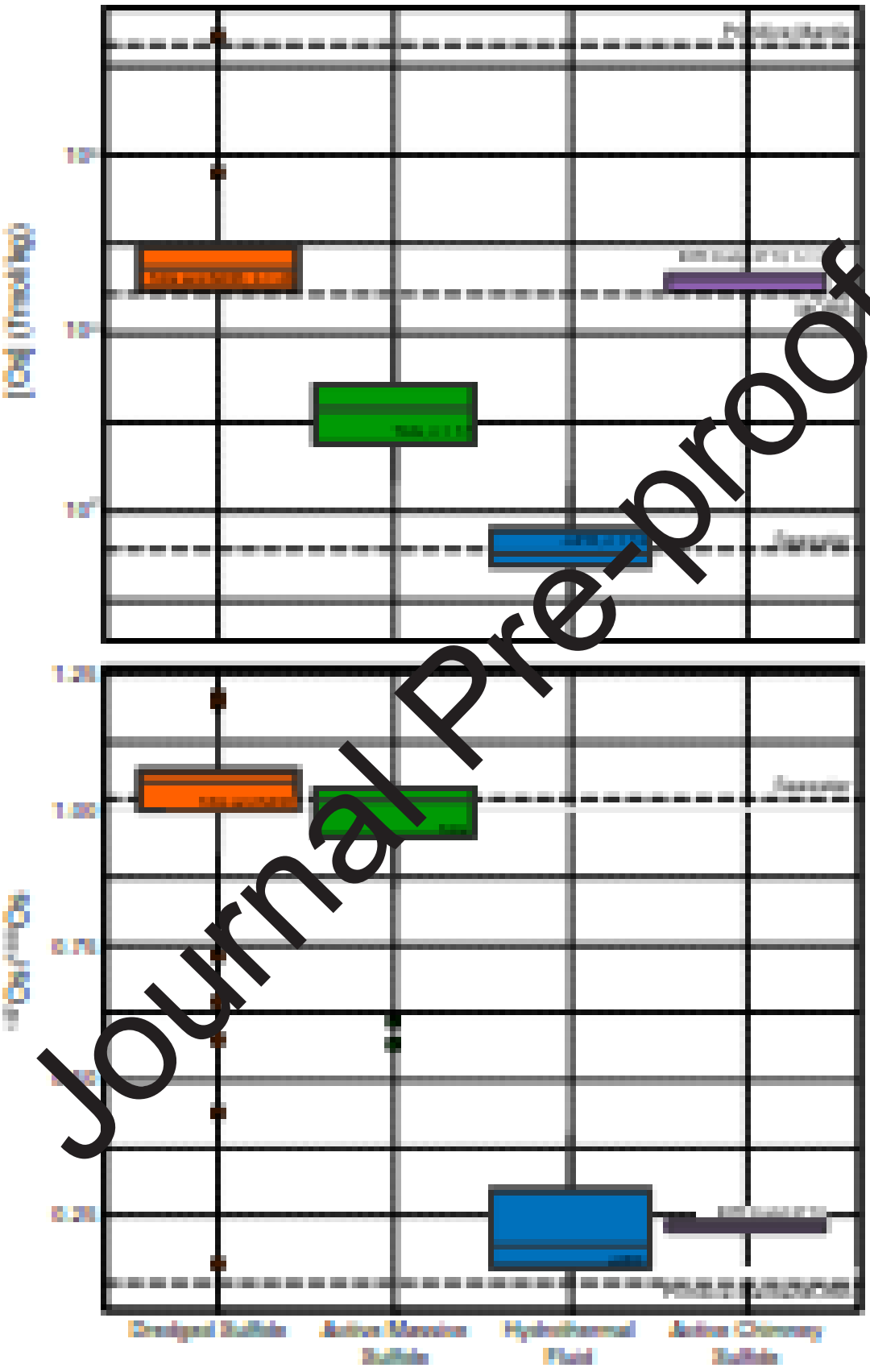

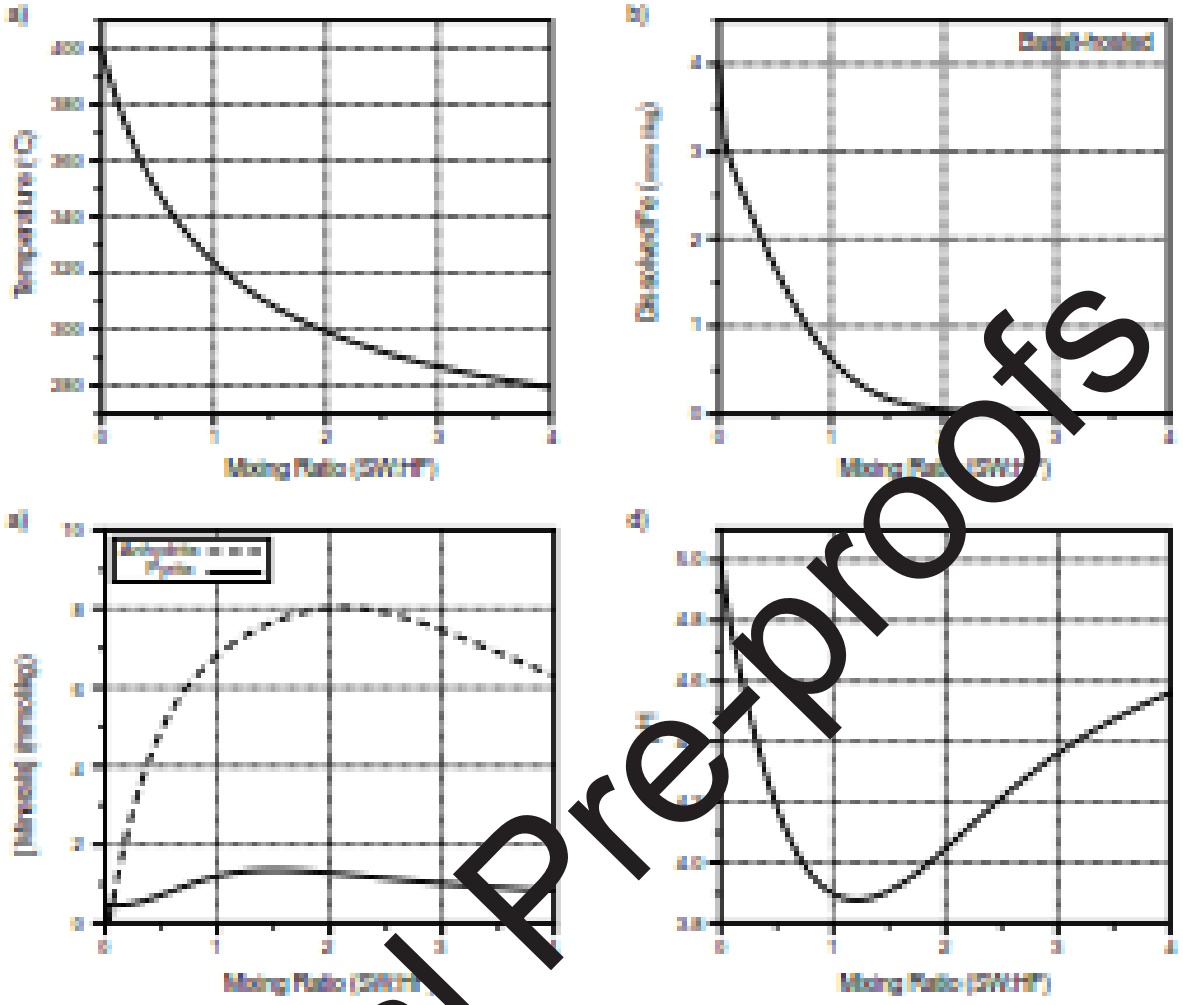

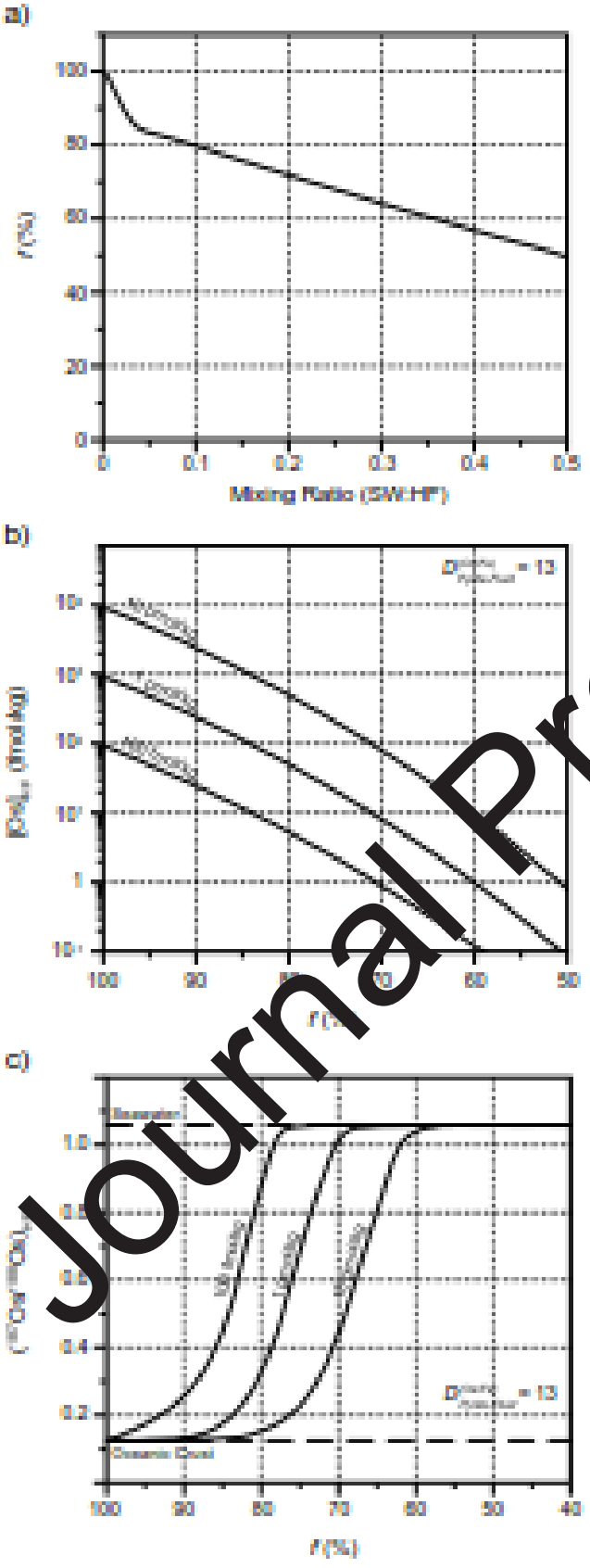

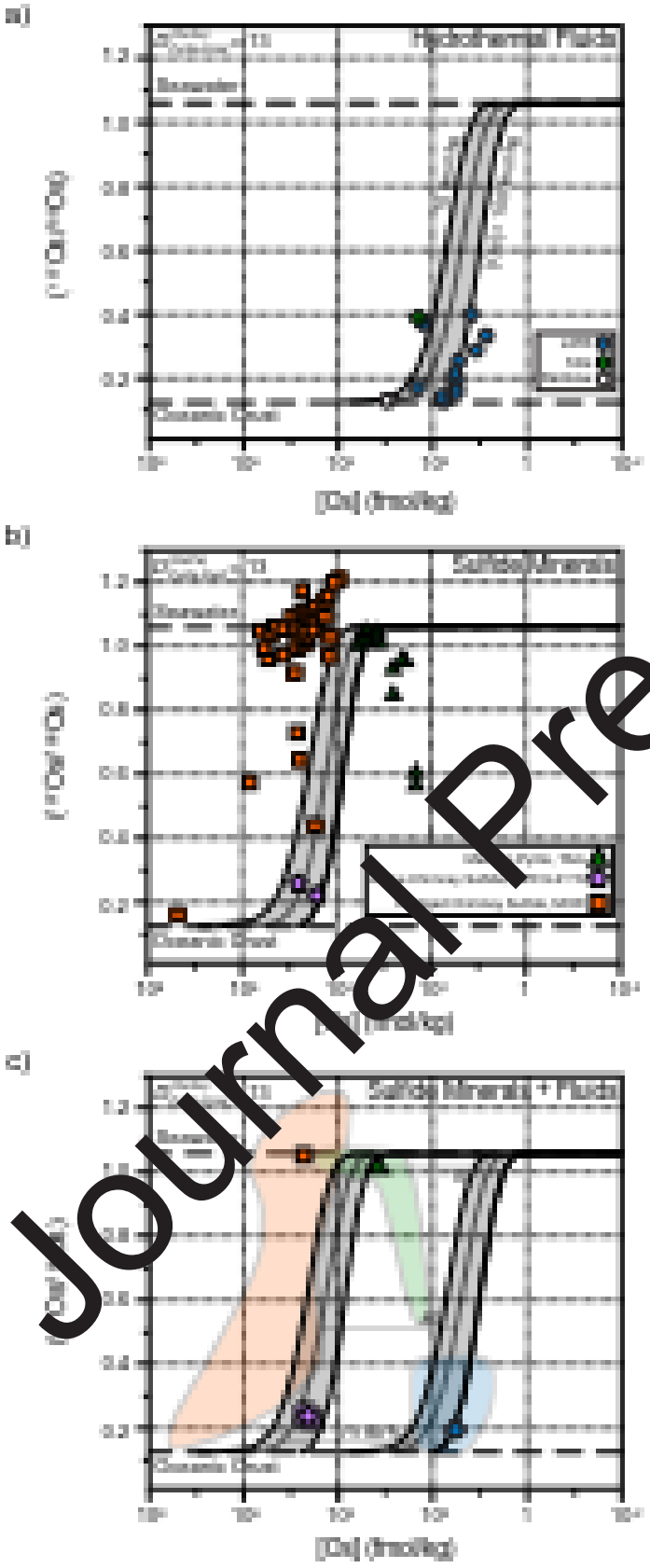

Declaration of interests

☒ The authors declare that they have no known competing financial interests or personal relationships that could have appeared to influence the work reported in this paper.

☐The authors declare the following financial interests/personal relationships which may be considered as potential competing interests: